Title

TOPAS-nBio validation for simulating water radiolysis and DNA damage under low-LET irradiation

Journal

Physics in Medicine and Biology, 66(17)

ISSN

0031-9155

Authors

Ramos-Méndez, J
LaVerne, JA
Domínguez-Kondo, N
et al.

Publication Date

2021-09-07

DOI

10.1088/1361-6560/ac1f39

Peer reviewed

HHS Public Access

Author manuscript

Phys Med Biol. Author manuscript; available in PMC 2022 September 03.

Published in final edited form as:

Phys Med Biol. ; 66(17): . doi:10.1088/1361-6560/ac1f39.

TOPAS-nBio validation for simulating water radiolysis and DNA damage under Low-LET irradiation

J Ramos-Méndez[1,*], **JA LaVerne**[2], **N Domínguez-Kondo**[3], **J Milligan**[4], **V Štěpán**[5], **K Stefanová**[5], **Y Perrot**[6], **C Villagrasa**[6], **W-G Shin**[7], **S Incerti**[8], **A McNamara**[9], **H Paganetti**[9], **J Perl**[10], **J Schuemann**[9], **B Faddegon**[1]

[1]Department of Radiation Oncology, University of California San Francisco, San Francisco, CA 94115, USA.

[2]Radiation Laboratory and Department of Physics, University of Notre Dame, Notre Dame, IN 46556, USA.

[3]Facultad de Ciencias Físico Matemáticas, Benemérita Universidad Autónoma de Puebla, Puebla 72000, MEX.

[4]Department of Basic Sciences, School of Medicine, Loma Linda University, Loma Linda, CA, 92350, USA.

[5]Department of Radiation Dosimetry, Nuclear Physics Institute of the Czech Academy of Sciences, Prague, Czech Republic.

[6]Laboratoire de Dosimétrie des Rayonnements Ionisants, Institut de Radioprotection et Sûreté Nucléaire, Fontenay aux Roses, BP. 17, 92262, France

[7]Department of Radiation Oncology, Seoul National University Hospital, Seoul 03080, Republic of Korea.

[8]Univ. Bordeaux, CNRS, CENBG, UMR 5797, F-33170 Gradignan, France

[9]Department of Radiation Oncology, Physics Division, Massachusetts General Hospital & Harvard Medical School, Boston, MA, USA.

[10]SLAC National Accelerator Laboratory, Menlo Park, CA, USA.

Abstract

The chemical stage of the Monte Carlo track-structure simulation code Geant4-DNA has been revised and validated. The root-mean-square (RMS) empirical parameter that dictates the displacement of water molecules after an ionization and excitation event in Geant4-DNA has been shortened to better fit experimental data. The pre-defined dissociation channels and branching ratios were not modified, but the reaction rate coefficients for simulating the chemical stage of water radiolysis were updated. The evaluation of Geant4-DNA was accomplished with TOPAS-nBio. For that, we compared predicted time-dependent G values in pure liquid water for $^{\bullet}OH$, e^{-}_{aq}, and H_2 with published experimental data. For H_2O_2 and $H^{\bullet}$, simulation of added scavengers at different concentrations resulted in better agreement with measurements.

[*]Corresponding author. Jose.RamosMendez@ucsf.edu.

In addition, DNA geometry information was integrated with chemistry simulation in TOPAS-nBio to realize reactions between radiolytic chemical species and DNA. This was used in the estimation of the yield of single-strand breaks (SSB) induced by ^{137}Cs γ-ray radiolysis of supercoiled pUC18 plasmids dissolved in aerated solutions containing DMSO. The efficiency of SSB induction by reaction between radiolytic species and DNA used in the simulation was chosen to provide the best agreement with published measurements.

An RMS displacement of 1.24 nm provided agreement with measured data within experimental uncertainties for time-dependent G values and under the presence of scavengers. SSB efficiencies of 24% and 0.5% for •OH and H•, respectively, led to an overall agreement of TOPAS-nBio results within experimental uncertainties. The efficiencies obtained agreed with values obtained with published non-homogeneous kinetic model and step-by-step Monte Carlo simulations but disagreed by 12% with published direct measurements. Improvement of the spatial resolution of the DNA damage model might mitigate such disagreement.

In conclusion, with these improvements, Geant4-DNA/TOPAS-nBio provides a fast, accurate, and user-friendly tool for simulating DNA damage under low LET irradiation.

1 Introduction.

A reliable way to study the underlying channels of radiobiological damage is mechanistic modeling. The modeling task is accomplished with Monte Carlo track-structure (MCTS) codes that have the capability of combining complex DNA geometry models with the stochastic processes of the interaction of ionizing radiation with matter and the subsequent non-homogeneous chemistry processes to produce initial DNA damage. MCTS codes specific for radiobiological applications include KURBUC (Nikjoo *et al* 2016), PARTRAC (Dingfelder *et al* 1999), Geant4-DNA (Incerti *et al* 2010a, 2010b, Bernal *et al* 2015), RITRACKS (Plante and Devroye 2017), RADAMOL (Štěpán and Davídková 2014), and TOPAS-nBio (Schuemann *et al* 2018). The reported results obtained with such codes demonstrate the usability of the Monte Carlo method to quantify DNA damage-induced at early stages following irradiation from first principles.

MCTS codes, being flexible mechanistic tools initially developed for liquid water calculations, have demonstrated acceptable accuracy in estimating DNA damage induced by ionizing radiation from first principles. However, many radiobiology-oriented MCTS codes overestimate the yields of •OH radical produced by fast electrons in liquid water within the nanosecond time scale (Kreipl *et al* 2009, Uehara and Nikjoo 2006, Ramos-Méndez *et al* 2018, Boscolo *et al* 2018). This inaccuracy might potentially mislead the interpretation of calculated DNA damage yields and hence requires benchmarking. In this work, we aim to reconcile MCTS by comparing simulated with experimentally measured yields from the literature for radiolytic species produced by fast electrons at the earliest times.

Experimental validation is paramount to determine the accuracy of the Monte Carlo method. A common approach among MCTS codes assumes that, from the physics perspective, liquid water is sufficient to represent biological tissue (Friedland *et al* 2017, Nikjoo *et al* 2016, Sakata *et al* 2019, Zhu *et al* 2020b). For this reason, MCTS validation relies upon the

comparison between calculated quantities with measurements performed in gas or liquid water (see e.g., (Burigo *et al* 2016, Kreipl *et al* 2009, Pimblott and LaVerne 1997)). Under low linear energy transfer (LET) irradiation, e.g., 0.4 keV/μm track-averaged LET for ^{137}Cs (Bruce *et al* 1963), the highest contribution to DNA lethal damage is caused by reactions with hydroxyl radicals produced in the radiolysis of water (e.g. > 70% for ^{60}Co, estimated with DNA plasmids pBR322 at scavenging capacities below ~5×10^8 s^{-1}) (Klimczak *et al* 1993). Therefore, thorough validation of the models used by MCTS to simulate the chemical stage in the radiolysis in water is crucial. This task has been accomplished typically by comparing calculated time-dependent yields in pure liquid water with measurements performed in solutes at different scavenging capacities. Subsequently, MCTS codes have been tuned to match the experimental yields at the earliest times available to date.

The accuracy of experimental measurements of radiolytic yields continuously improves. Nowadays, the most accurate picosecond-level measurements of radiolytic yields produced in liquid water by fast electrons have been performed with electron pulse radiolysis. The most recent measurements have determined reference G values (number of chemical species created or lost per 100 eV of energy deposit) for hydroxyl radicals (•OH) of 4.8 ± 0.2 molec./100 eV and solvated electron (e^-_{aq}) yields of 4.2±0.2 molec./100 eV after just 7 ps (El Omar *et al* 2011) (Wang *et al* 2018). These values are significantly lower than previous values used to calibrate Monte Carlo simulations (see e.g., (Tomita *et al* 1997, Kreipl *et al* 2009, Pimblott *et al* 1996, Uehara and Nikjoo 2006) and call for revisiting the input parameters of MCTS codes. A re-evaluation of such parameters has been mentioned for the radiation chemistry code IONLYS-IRT (Sanguanmith *et al* 2013, Sultana *et al* 2020); however, specific details of parameter adjustment were not reported.

On the other hand, to verify the accuracy of MCTS for radiobiology applications, sophisticated DNA models have been developed based on the whole cellular nucleus to identify and quantify clustered DNA strand breaks sites (Nikjoo *et al* 2016, Friedland *et al* 2017, Štěpán and Davídková 2014, Meylan *et al* 2017, Lampe *et al* 2018b, Sakata *et al* 2019, Zhu *et al* 2020a). The spatial resolution of experimental measurements at the cellular level is insufficient to validate Monte Carlo simulation outputs directly; for example, experimental techniques can still not resolve spatial distributions of individual DNA single-strand breaks (SSB) and double-strand breaks (DSB), and there is insufficient data about the structure and the radiation chemistry of chromatin. Thus, different assumptions have been made by different research groups to reconcile their MCTS results with experimental data, which impacts the accuracy of the codes. In particular, the scavenging capacity of the biological environment has been mimicked by limiting the time domain to a few nanoseconds. Moiseenko et al. (Moiseenko *et al* 1998) showed that this approach introduces 20%−30% differences in strand break yields compared to the explicit simulation of scavenger molecules uniformly distributed around the radiation spurs. Besides, the simulation of the chemical and biological mechanisms occurring within a cell is not a trivial task (Wardman 2020), and MCTS simulations have not yet utilized the corresponding models to simulate more reliable cellular conditions.

The selection of a less complex biological system than a cell would assist in providing relevant data to evaluate the accuracy of MCTS. Plasmids of DNA are a convenient example.

Experiments consisting of the irradiation of plasmids can be performed in a well-controlled environment with solutes of various scavenging capacities (Milligan *et al* 1996). Thus, under low LET irradiation, direct comparison with plasmid experiments provides a suitable way to validate directly MCTS radiochemistry capabilities. Comparison of MCTS with plasmid experiments considering direct and indirect damages has been performed in the past (Tomita *et al* 1998) (Fulford *et al* 2001) (Edel *et al* 2006).

In this work, we focus on the comparison of calculated versus published measured data to evaluate the accuracy of TOPAS-nBio. Parameters for modeling the radiation chemistry process of TOPAS-nBio were revisited, driven by the latest published experimental measurements of G values of radiation yield for fast electrons at the picosecond level. In that way, a reconciliation between measured and Monte Carlo modeled G values in liquid water was achieved. Then, we validated TOPAS-nBio for simulation of indirect damage of DNA. To this end, experimental setups of plasmids under low-LET irradiation reported in the literature were replicated with our validated Monte Carlo track-structure tool. Our benchmarked code provides a tool over which extended features regarding effects of temperature, compaction of DNA, oxygen concentration and other radiation chemistry processes may be implemented and evaluated.

2 Materials and methods.

The physics list comprises models describing the discrete transport of electrons in liquid water with no production cuts for secondary electrons, and all the interaction events are explicitly simulated. The selected models have been described extensively elsewhere (Incerti *et al* 2018, Shin *et al* 2019, Ramos-Méndez *et al* 2020). In brief, the physics list, encapsulated in the “G4EmDNAPhysics_option2” constructor, includes an elastic scattering model based on the partial wave theory and an inelastic scattering model based on the formalism of the complex dielectric response function of liquid water. For the latter model, four ionization shells and five discrete electronic excitation states are considered. In Geant4-DNA, after an ionization has taken place, the energy of the emitted secondary electron is calculated from the differential (in energy transfer) ionization cross section, which is described by the so-called Born ionization model. This model applies to weakly bound electrons in the liquid water molecule and adopts the dielectric response function formalism. In the case of K-shell ionization (of the oxygen atom), the atomic model Binary-encounter-Approximation-with-Exchange (BEAX) is used. Both models are described in more detail in Incerti et al (2018) and references therein. Models to simulate vibrational excitation and electron attachment processes are also included in the constructor.

The reaction kinetics is calculated with the independent reaction times method, IRT (Tachiya 1983, Clifford *et al* 1986, Green *et al* 1990, Pimblott *et al* 1991). The implementation in TOPAS-nBio is described elsewhere (Schuemann *et al* 2018, Ramos-Méndez *et al* 2020). The simulation of scavengers is performed with the continuum approximation (Pimblott *et al* 1991) where it is assumed that the scavenging molecules are uniformly distributed in the background. Then, the probability of chemical species potentially reacting with the background at time t is described by an exponential distribution given by $1 - \exp(-k[B]\ t)$, where the product of reaction rate k and scavenger concentration $[B]$, $k[B]$, is the scavenging

capacity of the background. Instantaneous scavenging within reaction distance R, at the time of chemical species creation, is performed with a probability given by $\exp(-4\pi R^3[B]/2)$ (Pimblott *et al* 1991). The reactions and rate constants used in this work are presented in table 1, obtained from (Pimblott 1992). These values originated from the National Institute of Standards and Technology (NIST) database (Buxton *et al* 1988), where each rate constant was evaluated for accuracy and consistency.

2.1 Validation of TOPAS-nBio for water radiolysis simulations for fast electrons.

To validate TOPAS-nBio, we revisit Geant4-DNA (version 10.6.p03) parameters for the simulation of the pre-chemical stage of water radiolysis previously reported (Kreipl *et al* 2009, Karamitros *et al* 2011, Ramos-Méndez *et al* 2018, Shin *et al* 2019). Prior to the dissociation of the ionized water molecules (H_2O^+), hole migration by electron correlation and electron relaxation (charge migration) results in a displacement of these molecules and their dissociation products from the place of energy transfer (Ogura and Hamill 1973, Despré *et al* 2015, Kuleff *et al* 2016). In Geant4-DNA, this process is considered by adding an isotropic displacement from where the ionization event occurred. The distance is sampled from a normal distribution with a given root-mean-square deviation (RMS). Due to the lack of measured data at the pre-chemical stage, the root-mean square (RMS) values (inherited from the PARTRAC code) are set to match measured yields of $^{\bullet}$OH radical available in 2009 (Kreipl *et al* 2009). In Table 2, the distances used in Geant4-DNA are described. In this work, the selection of empirical values $RMS^{H_2O^+}$ and $RMS^{H_2O^*}$ is driven by experimental G values for $^{\bullet}$OH radicals obtained at the picosecond time range for fast electrons reported in (Wang *et al* 2018). We increased the displacement distance in multiples of the mean separation between water molecules, 0.31 nm (Perkins 1986), to minimize the discrepancy with measured data. The branching ratios are kept unchanged, as reported in table 4 in (Shin *et al* 2019) and originally reported in (Kreipl *et al* 2009).

The thermalization of sub-excited electrons is simulated using a “one-step model” with displacement parameters obtained from the literature. The transport of each individual sub-excited electron is stopped once its kinetic energy is reduced to <10 eV. Later, in this one-step model, a solvated electron is placed at a distance (around the last interaction point) randomly sampled from a Gaussian distribution, with a standard deviation given by the data reported in (Ritchie *et al* 1994), with the correction factor described in (Shin *et al* 2019). The data from Ritchie et al, 1994, provided the best agreement with measured data of the time-dependent G-values for solvated electrons from (El Omar *et al* 2011) when using the physics list selected in this work. This model and other approaches to simulate the thermalization of solvated electrons have been discussed in detail elsewhere (Shin *et al* 2019).

The simulation setup consists of a homogenous liquid water box (1 g/cm^3 density) irradiated with monoenergetic electrons of 1 MeV. This setup is commonly used to simulate MCTS codes for fast electrons, as reported elsewhere (Pimblott and LaVerne 1997, Uehara and Nikjoo 2006, Ramos-Méndez *et al* 2018). Specifically, an isotropic electron source is positioned in the center of a cubic water phantom of 1 cm side. When the primary electron has lost more than 10 keV, the tracking of the electron is stopped, and it is removed from the

simulation. The secondary electrons are then followed until their kinetic energy is reduced at or below 10 eV, the low energy limit of the ELSEPA model (Shin et al 2018). After that, thermalization is simulated with the one-step model. The total energy deposited in the aqueous medium thus corresponds to the energy lost by the primary electron, which is at least 10 keV (Karamitros 2012). Immediately, the pre-chemical stage takes place, and the initial position of radiolytic products are obtained and input to the IRT method for the simulation of the chemical stage up to 10 μs.

A comparison with reference data for H_2, $H^{\bullet}$, and H_2O_2 was performed. For H_2, data was obtained from (Pastina *et al* 1999). The authors stated that reported G values are suitable for direct comparison with Monte Carlo simulations without scavengers. For H_2O_2 and $H^{\bullet}$, the scavenger system used in the experiments was replicated in our simulations. G values of H_2O_2 measured in solutions containing NO_3^- at a concentration of 25 mM, and CH_3OH at concentrations ranging from 10^{-3} – 10 M, were obtained from (Hiroki *et al* 2002). For $H^{\bullet}$, measured G values in solutions containing 1 mM of Br, 1 mM of NO_3^- and HCO_2^- at a concentration ranging from 10^{-2} – 1 M were obtained from (Huerta Parajon *et al* 2008). For the latter set of data, replicating the experiment, the calculated yield of $H^{\bullet}$ was estimated from the total yield of H_2 calculated with HCO_2^- subtracted from the total yield of H_2 calculated without HCO_2^- (Huerta Parajón 2010). The reactions used for simulations in the presence of scavengers are shown in table 1. The irradiation setup was the same as that used for pure liquid water simulations.

2.2 Validation of TOPAS-nBio for damage in supercoiled DNA plasmid.

The validation of DNA damage under low-LET irradiation was performed for the experimental conditions from plasmid DNA in aerobic aqueous solution irradiated with ^{137}Cs γ-rays, as reported in (Milligan *et al* 1993, Milligan and Ward 1994). A two-stage simulation was performed using condensed-history and track-structure Monte Carlo with TOPAS and TOPAS-nBio, respectively, as described below.

The first stage was used to determine the energy spectrum, at electronic equilibrium conditions, of secondary electrons set in motion by ^{137}Cs γ-rays interacting in a water phantom. For that, the TOPAS tool (Perl *et al* 2012, Faddegon *et al* 2020) version 3.5 was used to simulate a concentric system of two homogenous spherical water phantoms of 5 cm and 10 cm radius, respectively. The physics list used the constructor "G4EmStandardPhysics_option4" with a production cut for secondary electrons of 0.05 mm, extensively benchmarked for applications in medical physics (Arce *et al* 2021). An isotropic point source of monoenergetic γ-rays (662 keV) was positioned at the center, as shown in figure 1. We obtained the vertex kinetic energy spectrum (at the position of creation) of those secondary electrons that reached a phase space tallied on the surface of a 5 cm radius sphere. In total, 4×10^8 γ-rays were simulated.

The second stage consists of track-structure Monte Carlo simulations with TOPAS-nBio. The following assumptions are made for simulating the interactions of secondary electrons and reactions of chemical species with DNA molecules. All the medium, including the region occupied by the DNA geometry is made of liquid water. For biological targets, a canonical double helix B-DNA configuration is considered. The DNA sugar-phosphate

groups and nucleobases, represented as cut spheres in figure 1, are the main target of the radiation or chemical species to cause DNA damage. The spatial coordinates of the centroids of the semi-spheres corresponding to sugar-phosphate groups are included in the IRT method for the realization of reactions with the chemical species produced in the water radiolysis process. The coordinates are determined by the supercoiled path, which defines the plasmid DNA model (see below). DNA nucleobases are not included in the reaction kinetics because observed rate constants between chemical species and DNA are used (Tomita *et al* 1998, Perry *et al* 2020), but they are present for ionization/excitation interactions (see below). For the simulated time domain of the chemical stage (10^{-12}–10^{-4} s), the plasmid DNA model is assumed static. Accumulation of energy deposition of at least 17.5 eV in the sugar-phosphate volumes is considered to register an SSB from direct physical interactions (see (Lampe *et al* 2018a, Zhu *et al* 2020b) and references therein). Chemical species originated from radiolysis occurring within the regions occupied by the DNA semi-spheres are not included in the reaction kinetics and are eliminated upon creation, i.e., no DNA radiolysis is simulated.

For modeling indirect damage, a SSB is registered with specific efficiency after the reaction between $^{\bullet}$OH and DNA (as a whole) occurred (Önal *et al* 1988, Milligan *et al* 1993, Klimczak *et al* 1993). The reaction rate coefficient for the •OH+DNA reaction (table 1) depends on the scavenging capacity of the irradiated environment and is obtained from measured data reported elsewhere (Milligan et al 1996). For $H^{\bullet}$ and e^{-}_{aq}, constant reaction rates are used as obtained from (Buxton et al 1988). We estimate the DNA strand break efficiencies of $^{\bullet}$OH and $H^{\bullet}$ by minimization. We compare calculated to measured data applying a minimization algorithm using the Nelder-Mead method (Nelder and Mead 1965) to find the best efficiency values. For e^{-}_{aq}, no strand breaking in DNA is counted as it has not been observed experimentally (Jones and O'Neill 1991), but reactions with DNA are included as e^{-}_{aq} binds efficiently with nucleobases (Kumar et al 2019).

The DNA model is wrapped around supercoiled paths to reconstruct pUC18 plasmids (length of 2686 base-pairs length) utilizing DNAfabric (Meylan *et al* 2015). In a separate simulation, the geometric model of the pUC18 plasmid (Yanisch-Perron *et al* 1985) is constructed by the worm-like chain method and subsequent smoothing to base-pair level. First, the supercoiling of a circular plasmid represented by 91 linear segments is modeled using the elastic worm-like chain code developed by the group of A. Vologodskii (Vologodskii and Cozzarelli 1994, Huang *et al* 2001). The temperature is set to 298 K, the superhelical density to −0.06, and the step length to 500 ps. Resulting coarse configurations are converted to sets of 2686 equidistant points along a smooth path using an in-house code implementing the approach of Kümmerle and Pomplun (Kümmerle and Pomplun 2005). One sample supercoiled plasmid configuration is selected for the Monte Carlo simulation of DNA damage.

The plasmid is positioned multiple times inside a spherical water phantom of 0.5 μm radius. The positions and orientations of the plasmids are uniformly random. The sphere is centered in a cubic water box of 2 μm side. A volumetric electron source is uniformly distributed in the cubic box, including the sphere. The initial electron spectrum is calculated in the first stage using a condensed-history Monte Carlo, where the initial directions are set to

be isotropic (figure 1). In the experiment (Milligan *et al* 1993), the DNA is dissolved in an aerated solution containing DMSO. Thus, we simulated the scavenging behavior of that solution using the reaction rates shown in Table 1 for e^-_{aq} and $H^\bullet$ with O_2, using a concentration of 21% O_2 (0.27×10^{-3} mol dm^{-3}). We report the G value of SSBs using the same units of the experimental data (μmol J^{-1}) as a function of scavenging capacity for DMSO. In this way, measured results from (Perry et al 2021) performed with different scavenger can be included. The DMSO concentrations range from 0.5×10^{-4} to 1 mol dm^{-3} and the DNA concentration is 50 μg mL^{-1}. We estimated that nine pUC18 plasmids in the spherical phantom of 0.5 μm radius are equivalent to approximately 50 μg mL^{-1} of DNA concentration (50×10^{-6} g $mL^{-1} \times 10^3$ $L^{-1} \times$ mL /(2686 bp × 650 g mol^{-1} bp^{-1})] × $N_{av} \times 5.24 \times 10^{-16}$ L ≈ 9). Results for calculated SSB yields as a function of DNA concentration (from 10 – 200 μg mL^{-1}) for a concentration of 10^{-3} mol dm^{-3} DMSO are also reported. Finally, the yield of SSB and DSB as a function of $^\bullet$OH scavenging capacity (from 7.1×10^5 – 7.1×10^9 s^{-1}) are reported. A DSB was scored when there was no more than a 10 base-pair distance between at least two SSB's occurring in opposite DNA strands. The total number of simulation jobs with independent random number seeds were 200 to 500, achieving statistical uncertainties from 0.7% to 5% (one standard deviation) for the simulation with the lowest and highest DMSO concentration, respectively. On average, 1150±80 primary histories are generated in each simulation job to achieve an absorbed dose of 30 Gy in the spherical phantom. In a systematic study (not shown) we found that 30 Gy absorbed dose provided a reasonable computing memory and speed, resulting from the number of primary yields used in the IRT and their processing time. The simulations take between 3 to 6 minutes to complete on a single core of a 2.7 GHz 12-Core Intel Xeon E4.

3 Results.

3.1 Time-dependent G values for fast electrons.

It was found that a distance of four water molecule's mean separation distances, 1.24 nm, for both $RMS^{H_2O^+}$ and $RMS^{H_2O^*}$ reproduced the measured time-dependent G values for $^\bullet$OH radicals. The G values using that value are shown in figure 2. In the top row of the figure, the calculated G value in pure liquid water for $^\bullet$OH, e^-_{aq} and H_2 are displayed in individual panels, along with experimental data. The agreement for the three sets of data along all the time domains was within one standard deviation of experimental measurements. In the bottom row of figure 2, the G value for H_2O_2 and $H^\bullet$ is displayed in each panel. As depicted, the time-dependent G values calculated in pure liquid water (solid line) did not reproduce the behavior of the experimental yields for H_2O_2 (empty circles) and $H^\bullet$ (filled triangles). However, the simulations considering the scavengers used in the experiments (squares connected by dashed lines) agreed within one standard deviation of the experimental data.

3.2 DNA damage in plasmid geometries.

In figure 3, calculated and measured SSB yields as a function of $^\bullet$OH scavenging capacity are shown. The estimated efficiencies for $^\bullet$OH and $H^\bullet$ are 24% and 0.5%, respectively. These values are used in all the following results. As depicted, the calculated SSB yields reproduced the measured data from pUC18 irradiations along with the considered DMSO

concentrations reasonably well. The yields included the G(SSB) produced by direct effects, which resulted in $1.77\pm0.01 \times 10^{-6}$ μmol/J for the geometrical DNA model used in this work. Figure 4 shows G(SSB) as a function of the DNA concentration. The slopes of linear regression fitting to both calculated and measured data agreed within 1%±0.8%. Finally, calculated DBS as a function of $^{\bullet}OH$ scavenging capacity reproduced the behavior of measured yields well as shown in figure 5.

4 Discussion.

In this work, TOPAS-nBio was applied to simulate water radiolysis and DNA damage under low-LET irradiation. The simulation of the reaction kinetics was performed with the IRT method, providing a fast and reliable tool to assist in investigating the biological effect of the interaction of ionizing radiation at the early stages.

Calculated G values at the picosecond stage agreed within experimental errors of published direct measurements of $^{\bullet}OH$ and e^{-}_{aq} performed in pure liquid water. The temporal evolution of the G values simulated up to the microsecond time stage was also well reproduced by TOPAS-nBio for $^{\bullet}OH$, e^{-}_{aq}, and H_2. To obtain such an agreement we adjusted the RMS of the displacement of ionized and excited water molecules caused by charge migration. Oscillating charge migration is expected to happen a few femtoseconds after an energy transfer event, hence challenging its experimental observation given the short period of time (Kuleff *et al* 2016). Thus, RMS values have been empirically adjusted in other Monte Carlo track-structure codes due to the lack of corresponding measured data (Kreipl *et al* 2009, Cobut *et al* 1998, Tomita *et al* 1997, Uehara and Nikjoo 2006). The RMS obtained in this work (1.24 nm), shorter than Geant4-DNA's default value (2 nm), increased the chance of contact reactions at the earliest times producing lower yields of $^{\bullet}OH$ radical. For $^{\bullet}OH$ radicals at 7 ps, this modification represented a reduction from 5.0 molecules per 100 eV (Ramos-Mendez et al., 2020) to 4.7 molecules per 100 eV (the measure data show 4.7±0.2 molecules per 100 eV (Wang *et al* 2018)). Geant4-DNA being a radiation transport code is not currently capable of simulating molecular dynamics of water molecules. Thus, effects like the binding of water molecules to biomolecules (DNA, proteins or lipids) that in principle affect the RMS displacement (see e.g., Shweta and Sen 2018), cannot be studied in detail at this point with our code. For e^{-}_{aq}, this parameter had a negligible effect as the products of auto-ionization that followed a dissociation event were handled by the one-step thermalization method (Shin *et al* 2019).

While it is a common practice, the comparison between time-dependent product yields calculated in pure liquid water and measured data under the presence of scavengers deviated from each other and should be avoided. In this work, two sets of data were selected to demonstrate this point. The temporal evolution of H_2O_2 and $H^{\bullet}$ reproduced the measured data within experimental errors only when the yields were calculated in the presence of scavengers. However, a more comprehensive evaluation of TOPAS-nBio under a wide range of scavengers, scavenger concentrations, and radiation qualities was outside the scope of this work and it is the subject of future work. A selection of radiobiologically relevant scavengers should precede that task given the scope of TOPAS-nBio.

On the other hand, for DNA damage simulations an encouraging agreement was found between calculated yields of SSB and DSB with measured data for low-LET radiation on a base-pair level. A limitation of the applicability of IRT for smaller scales (e.g., including adenine, thymine, cytosine, and guanine nucleobases or atomic components) could be expected. Bluett and Green demonstrated (Bluett and Green 2006) that at such proximity, multiple reactive centers in the sugar-base system might occur, so the reaction rate between a reaction pair is affected by the presence of static neighboring species. The IRT method assumes that reactions between pairs occur in isolation, thus, the IRT method may give inaccurate results. Nevertheless, the use of observed reaction rates in this work provided a base-pair level resolution, which resulted in a general agreement within experimental uncertainties.

The estimated SSB efficiencies from the Monte Carlo data included a highly detailed plasmid DNA geometrical model. The estimated efficiency of 24% for SSB induction for •OH was within previously reported values between 24% to 44% obtained with cylindrical non-homogeneous kinetic model (Milligan *et al* 1993, Udovičić *et al* 1994, Klimczak *et al* 1993). In that model, however, a homogenous cylindrical model representing a straight DNA segment was considered, which differed from the more detailed supercoiling DNA representation facilitated by TOPAS-nBio. For H•, the efficiency of 0.5% provided the best agreement at higher scavenger concentrations. This value was close to the 0.81% calculated by (Aydogan et al 2008). The differences are subtle and could be attributed to the different Monte Carlo codes used used by these authors. In their model, the authors used a straight linear DNA segment of 38 bp, with atomic resolution and multiple reactions sites on a base pair. However, our calculated efficiency was 12% higher than that measured experimentally (Milligan *et al* 1993). This difference may be due to the limited resolution of our model, justified by the use of the variable rate coefficient for •OH + DNA, which disregards the individual reactions with nucleobases and other components. The reaction of •OH with nucleobases is in general several times faster than the reaction of •OH with deoxyribose (Buxton *et al* 1988). Thus, by including reactions with DNA bases, an increment in the number of •OH reactions is expected, which might lead to a lower SSB efficiency. For that, reaction rate constants obtained in a B-DNA structure instead of an aqueous solution of DNA are needed. From the computational point of view, an effort of our group to find ways to extend the IRT method to handle DNA bases was reported in (Tran *et al* 2021). On the other hand, our estimation of the direct effect assumed an energy threshold for accumulated energy depositions of at least 17.5 eV, which produced 28% fewer SSB compared to, e.g., the 5–37.5 eV linear ramp threshold shown elsewhere (Zhu *et al* 2020b). A more suitable selection of the energy threshold must consider the transport of low energy electrons below 15 eV (avoiding the one-step thermalization model), which can induce DNA damage, as shown experimentally by (Alizadeh *et al* 2015). In that regard, an extended physics package which improves the detail in the pre-chemical stage for handling Auger electrons and electron capture will be soon made available in Geant4 (Shin et al., 2021 under review). Experimentally, a dependence with the scavenging capacity of the SSB induction efficiency was further observed (Önal *et al* 1988). Even though we used a single constant value as a first approach, the assumptions made in this work were sufficient to reproduce the behavior of scavenging dependence of DSB yields measured for different plasmids.

5 Conclusions.

In this work, TOPAS-nBio was validated for simulating water radiolysis in liquid water and DNA damage for plasmids at low LET irradiation. Satisfactory agreement within experimental uncertainties was obtained, reconciling Monte Carlo calculations of water radiolysis from $^{\bullet}OH$ and e^{-}_{aq} yields at the picosecond level. For pUC18 plasmids irradiated by ^{137}Cs γ-rays, calibration via the SSB induction efficiency was consistent with published efficiency values, leading to agreement with measure data within experimental uncertainties. TOPAS-nBio facilitated the implementation of experimental conditions of DNA irradiations including DNA geometry, source quality, prescribed dose, chemical parameters, and scavengers, exploiting the full potential of Geant4-DNA. As a result, an accurate, fast, and user-friendly Monte Carlo framework is provided by TOPAS-nBio/Geant4-DNA to evaluate DNA damage from first principles.

Acknowledgments

This work was supported by NIH/NCI R01 CA187003 (TOPAS-nBio). V.Š. and K.S. were supported by the Czech Science Foundation project no. 17-03403Y. N.D-K. is a doctoral student from Programa de Doctorado en Ciencias Física Aplicada, Benemérita Universidad Autónoma de Puebla and received fellowship 2019-000002-01NACF-05024 from CONACYT, México.

References.

Alizadeh E, Orlando TM and Sanche L 2015 Biomolecular damage induced by ionizing radiation: The direct and indirect effects of low-energy electrons on DNA Annu. Rev. Phys. Chem 66 379–98 [PubMed: 25580626]

Arce P, Bolst D, Bordage M, Brown JMC, Cirrone P, Cortés-Giraldo MA, Cutajar D, Cuttone G, Desorgher L, Dondero P, Dotti A, Faddegon B, Fedon C, Guatelli S, Incerti S, Ivanchenko V, Konstantinov D, Kyriakou I, Latyshev G, Le A, Mancini-Terracciano C, Maire M, Mantero A, Novak M, Omachi C, Pandola L, Perales A, Perrot Y, Petringa G, Quesada JM, Ramos-Méndez J, Romano F, Rosenfeld AB, Sarmiento LG, Sakata D, Sasaki T, Sechopoulos I, Simpson EC, Toshito T and Wright DH 2021 Report on G4-Med, a Geant4 benchmarking system for medical physics applications developed by the Geant4 Medical Simulation Benchmarking Group Med. Phys 48 19–56 Online: https://onlinelibrary.wiley.com/doi/abs/10.1002/mp.14226 [PubMed: 32392626]

Aydogan B, Bolch WE, Swarts SG, Turner JE and Marshall DT 2008 Monte Carlo Simulations of Site-Specific Radical Attack to DNA Bases Radiat. Res 169 223–31 [PubMed: 18220458]

Bartels DM, Cook AR, Mudaliar M and Jonah CD 2000 Spur decay of the solvated electron in picosecond radiolysis measured with time-correlated absorption spectroscopy J. Phys. Chem. A 104 1686–91

Bernal MA, Bordage MC, Brown JMC, Davídková M, Delage E, El Bitar Z, Enger SA, Francis Z, Guatelli S, Ivanchenko VN, Karamitros M, Kyriakou I, Maigne L, Meylan S, Murakami K, Okada S, Payno H, Perrot Y, Petrovic I, Pham QT, Ristic-Fira A, Sasaki T, Štěpán V, Tran HN, Villagrasa C and Incerti S 2015 Track structure modeling in liquid water: A review of the Geant4-DNA very low energy extension of the Geant4 Monte Carlo simulation toolkit. Phys. Med 31 861–74 Online: http://www.sciencedirect.com/science/article/pii/S1120179715010042 [PubMed: 26653251]

Bluett VM and Green NJB 2006 Competitive diffusion-influenced reaction of a reactive particle with two static sinks J. Phys. Chem. A 110 4738–52 [PubMed: 16599442]

Boscolo D, Krämer M, Durante M, Fuss MC and Scifoni E 2018 TRAX-CHEM: A pre-chemical and chemical stage extension of the particle track structure code TRAX in water targets Chem. Phys. Lett 698 11–8 Online: 10.1016/j.cplett.2018.02.051

Bruce WR, Pearson ML and Freedhoff HS 1963 The Linear Energy Transfer Distributions Resulting from Primary and Scattered X-Rays and Gamma Rays with Primary HVL's from 1.25 mm Cu to 11

mm Pb Radiat. Res 19 606 Online: https://www.jstor.org/stable/3571481?origin=crossref [PubMed: 14062234]

Burigo L, Pshenichnov I, Mishustin I, Hilgers G and Bleicher M 2016 Distributions of deposited energy and ionization clusters around ion tracks studied with Geant4 toolkit Phys. Med. Biol 61 3698–711 Online: http://stacks.iop.org/0031-9155/61/i=10/a=3698?key=crossref.6d36b15fba7d535b14de38a5fc3a9b1e [PubMed: 27081911]

Buxton GV, Greenstock CL, Helman WP and Ross AB 1988 Critical Review of rate constants for reactions of hydrated electrons, hydrogen atoms and hydroxyl radicals in Aqueous Solution J. Phys. Chem. Ref. Data 17 513–886

Clifford P, Green NJB, Oldfield MJ, Pilling MJ and Pimblott SM 1986 Stochastic Models of Multi-species Kinetics in Radiation-induced Spurs J. Chem. Soc., Faraday Trans 182 2673–89

Cobut V, Frongillo Y, Patau JP, Goulet T, Fraser MJ and Jay-Gerin JP 1998 Monte Carlo simulation of fast electron and proton tracks in liquid water - I. Physical and physicochemical aspects Radiat. Phys. Chem 51 229–43

Despré V, Marciniak A, Loriot V, Galbraith MCE, Rouzée A, Vrakking MJJ, Lépine F and Kuleff AI 2015 Attosecond hole migration in benzene molecules surviving nuclear motion J. Phys. Chem. Lett 6 426–31 [PubMed: 26261959]

Dingfelder M, Hantke D, Inokuti M and Paretzke HG 1999 Electron inelastic-scattering cross sections in liquid water Radiat. Phys. Chem 53 1–18

Edel S, Terrissol M, Peudon A, Kümmerle E and Pomplun E 2006 Computer simulation of strand break yields in plasmid pBR322: DNA damage following 125I decay Radiat. Prot. Dosimetry 122 136–40 [PubMed: 17185311]

Faddegon B, Ramos-Méndez J, Schuemann J, McNamara A, Shin J, Perl J and Paganetti H 2020 The TOPAS tool for particle simulation, a Monte Carlo simulation tool for physics, biology and clinical research Phys. Medica 72 114–21 Online: 10.1016/j.ejmp.2020.03.019

Friedland W, Schmitt E, Kundrát P, Dingfelder M, Baiocco G, Barbieri S and Ottolenghi A 2017 Comprehensive track-structure based evaluation of DNA damage by light ions from radiotherapy-relevant energies down to stopping Sci. Rep 7 45161 Online: http://www.nature.com/articles/srep45161 [PubMed: 28345622]

Fulford J, Nikjoo H, Goodhead DT and O'Neill P 2001 Yields of SSB and DSB induced in DNA by Al K ultrasoft X-rays and α-particles: comparison of experimental and simulated yields Int. J. Radiat. Biol 77 1053–66 Online: http://informahealthcare.com/doi/abs/10.1080/09553000110069308 [PubMed: 11682010]

Green NJB, Pilling MJ and Clifford P 1990 Stochastic Modeling of Fast Kinetics in a Radiation Track Society 94 251–8 Online: http://pubs.acs.org/doi/abs/10.1021/j100364a041

Hiroki A, Pimblott SM and Laverne JA 2002 Hydrogen peroxide production in the radiolysis of water with high radical scavenger concentrations J. Phys. Chem. A 106 9352–8

Huang J, Schlick T and Vologodskii A 2001 Dynamics of site juxtaposition in supercoiled DNA Proc. Natl. Acad. Sci. U. S. A 98 968–73 [PubMed: 11158579]

Huerta Parajón M 2010 HYDROGEN ATOM FORMATION IN THE GAMMA AND HEAVY ION RADIOLYSIS OF AQUEOUS SYSTEMS A thesis submitted to The University of Manchester for the (The University of Manchester)

Huerta Parajon M, Rajesh P, Mu T, Pimblott SM and LaVerne JA 2008 H atom yields in the radiolysis of water Radiat. Phys. Chem 77 1203–7

Incerti S, Baldacchino G, Bernal M, Capra R, Champion C, Francis Z, GuÈye P, Mantero A, Mascialino B, Moretto P, Nieminen P, Villagrasa C and Zacharatou C 2010a THE Geant4-DNA project Int. J. Model. Simulation, Sci. Comput 1 157–78

Incerti S, Ivanchenko A, Karamitros M, Mantero A, Moretto P, Tran HN, Mascialino B, Champion C, Ivanchenko VN, Bernal M a, Francis Z, Villagrasa C, Baldacchin G, Guèye P, Capra R, Nieminen P and Zacharatou 2010b Comparison of GEANT4 very low energy cross section models with experimental data in water. Med. Phys 37 4692–708 [PubMed: 20964188]

Incerti S, Kyriakou I, Bernal MA, Bordage MC, Francis Z, Guatelli S, Ivanchenko V, Karamitros M, Lampe N, Lee SB, Meylan S, Min CH, Shin WG, Nieminen P, Sakata D, Tang N, Villagrasa C, Tran HN and Brown JMC 2018 Geant4-DNA example applications for track structure simulations

in liquid water: A report from the Geant4-DNA Project Med. Phys 45 e722–39 Online: http://doi.wiley.com/10.1002/mp.13048

Jones GDD and O'Neill P 1991 Kinetics of radiation-induced Strand break formation in single-stranded pyrimidine polynucleotides in the presence and absence of oxygen; a time-resolved light-scattering study Int. J. Radiat. Biol 59 1127–45 [PubMed: 1675234]

Karamitros M, Mantero A, Incerti S, Friedland W, Baldacchino G, Barberet P, Bernal M, Capra R, Champion C, El Bitar Z, Francis Z, Gueye P, Ivanchenko A, Ivanchenko V, Kurashige H, Mascialino B, Moretto P, Nieminen P, Santin G, Seznec H, Tran HN, Villagrasa C and Zacharatou C 2011 Modeling Radiation Chemistry in the Geant4 Toolkit Prog. Nucl. Sci. Technol 2 503–8 Online: http://www.aesj.or.jp/publication/pnst002/data/503-508.pdf

Karamitros M 2012 Extension de l'outil Monte Carlo généraliste Geant4 pour la simulation de la radiolyse de l'eau dans le cadre du projet Geant4-DNA [Doctoral dissertation, L'Université Bordeaux 1] page 164: http://www.theses.fr/2012BOR14629.

Klimczak U, Ludwig DC, Mark F, Rettberg P and Schulte-Frohlinde D 1993 Irradiation of plasmid and phage DNA in water-alcohol mixtures: Strand breaks and lethal damage as a function of scavenger concentration Int. J. Radiat. Biol 64 497–510 [PubMed: 7902389]

Kreipl MS, Friedland W and Paretzke HG 2009 Time- and space-resolved Monte Carlo study of water radiolysis for photon, electron and ion irradiation Radiat. Environ. Biophys 48 11–20 Online: http://link.springer.com/10.1007/s00411-008-0194-8 [PubMed: 18949480]

Kuleff AI, Kryzhevoi NV., Pernpointner M and Cederbaum LS 2016 Core Ionization Initiates Subfemtosecond Charge Migration in the Valence Shell of Molecules Phys. Rev. Lett 117 1–5

Kumar A, Becker D, Adhikary A and Sevilla MD 2019 Reaction of electrons with dna: Radiation damage to radiosensitization Int. J. Mol. Sci 20

Kümmerle EA and Pomplun E 2005 A computer-generated supercoiled model of the pUC19 plasmid Eur. Biophys. J 34 13–8 Online: http://link.springer.com/10.1007/s00249-004-0431-2 [PubMed: 15300338]

Lampe N, Karamitros M, Breton V, Brown JMC, Kyriakou I, Sakata D, Sarramia D and Incerti S 2018a Mechanistic DNA damage simulations in Geant4-DNA part 1: A parameter study in a simplified geometry Phys. Medica 48 135–45 Online: 10.1016/j.ejmp.2018.02.011

Lampe N, Karamitros M, Breton V, Brown JMC, Sakata D, Sarramia D and Incerti S 2018b Mechanistic DNA damage simulations in Geant4-DNA Part 2: Electron and proton damage in a bacterial cell Phys. Medica 48 146–55 Online: 10.1016/j.ejmp.2017.12.008

Laverne JA 2000 OH Radicals and Oxidizing Products in the Gamma Radiolysis of Water Source Radiat. Res. Radiat. Res. Gamma Radiolysis Water. Radiat. Res 53–196 Online: http://www.jstor.org/stable/3580071

Ma J, Laverne JA and Mostafavi M 2015 Scavenging the Water Cation in Concentrated Acidic Solutions J. Phys. Chem. A 119 10629–36 [PubMed: 26449261]

Meylan S, Incerti S, Karamitros M, Tang N, Bueno M, Clairand I and Villagrasa C 2017 Simulation of early DNA damage after the irradiation of a fibroblast cell nucleus using Geant4-DNA Sci. Rep 7 1–15 [PubMed: 28127051]

Meylan S, Vimont U, Incerti S, Clairand I and Villagrasa C 2015 Geant4-DNA simulations using complex DNA geometries generated by the DnaFabric tool Comput. Phys. Commun

Milligan JR, Aguilera JA and Ward JF 1993 Variation of Single-Strand Break Yield with Scavenger Concentration for Plasmid DNA Irradiated in Aqueous Solution vol 133 Online: http://www.jstor.org/stable/3578350?origin=crossref

Milligan JR and Ward JF 1994 Yield of single-strand breaks due to attack on DNA by Scavenger-derived radicals Radiat. Res 137 295–9 [PubMed: 8146271]

Milligan JR, Wu CCL, Ng JYY, Aguilera JA and Ward JF 1996 Characterization of the reaction rate coefficient of DNA with the hydroxyl radical Radiat. Res 146 510–3 Online: http://www.jstor.org/stable/3579551 [PubMed: 8896577]

Moiseenko VV, Hamm RN, Waker AJ and Prestwich WV. 1998 The cellular environment in computer simulations of radiation-induced damage to dna Radiat. Environ. Biophys 37 167–72 [PubMed: 9840485]

Nelder JA and Mead R 1965 A Simplex Method for Function Minimization Comput. J 7 308–13 Online: https://academic.oup.com/comjnl/article-lookup/doi/10.1093/comjnl/8.1.27

Nikjoo H, Emfietzoglou D, Liamsuwan T, Taleei R, Liljequist D and Uehara S 2016 Radiation track, DNA damage and response—a review Reports Prog. Phys 79 116601 Online: http://stacks.iop.org/0034-4885/79/i=11/a=116601?key=crossref.97c4492091d158513ac8241fafa018bf

Ogura H and Hamill WH 1973 Positive hole migration in pulse-irradiated water and heavy water J. Phys. Chem 77 2952–4

El Omar AK, Schmidhammer U, Jeunesse P, Larbre JP, Lin M, Muroya Y, Katsumura Y, Pernot P and Mostafavi M 2011 Time-dependent radiolytic yield of OH• radical studied by picosecond pulse radiolysis J. Phys. Chem. A 115 12212–6 Online: http://pubs.acs.org/doi/pdf/10.1021/jp208075v [PubMed: 21970432]

Önal AM, Lemaire DGE, Bothe E and Schulte-Frohlinde D 1988 γradiolysis of poly(a) in aqueous solution: Efficiency of Strand break formation by primary water radicals Int. J. Radiat. Biol 53 787–96

Pastina B and LaVerne JA 1999 Hydrogen Peroxide Production in the Radiolysis of Water with Heavy Ions J. Phys. Chem. A 103 1592–7 Online: http://pubs.acs.org/doi/abs/10.1021/jp984433o

Pastina B, Laverne JA and Pimblott SM 1999 Dependence of Molecular Hydrogen Formation in Water on Scavengers of the Precursor to the Hydrated Electron J. Phys. Chem. A 103 5841–6 Online: https://pubs.acs.org/doi/pdf/10.1021/jp991222q

Perkins SJ 1986 Protein volumes and hydration effects. The calculations of partial specific volumes, neutron scattering matchpoints and 280-nm absorption coefficients for proteins and glycoproteins from amino acid sequences Eur. J. Biochem 157 169–80 Online: http://www.ncbi.nlm.nih.gov/pubmed/3709531 [PubMed: 3709531]

Perl J, Shin J, Schümann J, Faddegon B and Paganetti H 2012 TOPAS: An innovative proton Monte Carlo platform for research and clinical applications Med. Phys 39 6818–37 Online: http://doi.wiley.com/10.1118/1.4758060 [PubMed: 23127075]

Perry CC, Ramos-Méndez J and Milligan JR 2021 Boronated Condensed DNA as a Heterochromatic Radiation Target Model Biomacromolecules acs.biomac.1c00106 Online: https://pubs.acs.org/doi/10.1021/acs.biomac.1c00106

Perry CC, Ramos-Méndez J and Milligan JR 2020 DNA condensation with a boron-containing cationic peptide for modeling boron neutron capture therapy Radiat. Phys. Chem 166 108521 Online: https://linkinghub.elsevier.com/retrieve/pii/S0969806X19311417

Pimblott SM 1992 Investigation of various factors influencing the effect of scavengers on the radiation chemistry following the high-energy electron radiolysis of water J. Phys. Chem 96 4485–91 Online: https://pubs.acs.org/doi/pdf/10.1021/j100190a066

Pimblott SM and LaVerne JA 1997 Stochastic Simulation of the Electron Radiolysis of Water and Aqueous Solutions J. Phys. Chem. A 101 5828–38 Online: http://pubs.acs.org/doi/abs/10.1021/jp970637d

Pimblott SM, LaVerne JA, Bartels DM and Jonah CD 1996 Reconciliation of Transient Absorption and Chemically Scavenged Yields of the Hydrated Electron in Radiolysis J. Phys. Chem 100 9412–5 Online: https://pubs.acs.org/doi/pdf/10.1021/jp960816f

Pimblott SM, Pilling MJ and Green NJB 1991 Stochastic models of spur kinetics in water Int. J. Radiat. Appl. Instrumentation Part 37 377–88

Plante I and Devroye L 2017 Considerations for the independent reaction times and step-by-step methods for radiation chemistry simulations Radiat. Phys. Chem 139 157–72 Online: 10.1016/j.radphyschem.2017.03.021

Ramos-Méndez J, Domínguez-Kondo N, Schuemann J, McNamara A, Moreno-Barbosa E and Faddegon B 2020 LET-Dependent Intertrack Yields in Proton Irradiation at Ultra-High Dose Rates Relevant for FLASH Therapy Radiat. Res 194 5–7 Online: https://bioone.org/journals/radiation-research/volume-194/issue-4/RADE-20-00084.1/LET-Dependent-Intertrack-Yields-in-Proton-Irradiation-at-Ultra-High/10.1667/RADE-20-00084.1.full

Ramos-Méndez J, Perl J, Schuemann J, McNamara A, Paganetti H and Faddegon B 2018 Monte Carlo simulation of chemistry following radiolysis with TOPAS-nBio Phys. Med. Biol 63 105014 Online: http://iopscience.iop.org/article/10.1088/1361-6560/aac04c [PubMed: 29697057]

Ramos-Méndez J, Shin W, Karamitros M, Domínguez-Kondo J, Tran NH, Incerti S, Villagrasa C, Perrot Y, Štěpán V, Okada S, Moreno-Barbosa E and Faddegon B 2020 Independent reaction times method in Geant4-DNA: Implementation and performance Med. Phys 47 5919–30 Online: https://onlinelibrary.wiley.com/doi/10.1002/mp.14490 [PubMed: 32970844]

Ritchie RH, Hamm RN, Turner JE and Bolch WE 1994 Interactions of Low-Energy Electrons with Condensed Matter: Relevance for Track Structure Computational Approaches in Molecular Radiation Biology (Boston, MA: Springer US) pp 33–47 Online: http://link.springer.com/10.1007/978-1-4757-9788-6_4

Sakata D, Lampe N, Karamitros M, Kyriakou I, Belov O, Bernal MA, Bolst D, Bordage M-CC, Breton V, Brown JMC, Francis Z, Ivanchenko V, Meylan S, Murakami K, Okada S, Petrovic I, Ristic-Fira A, Santin G, Sarramia D, Sasaki T, Shin W-GG, Tang N, Tran HN, Villagrasa C, Emfietzoglou D, Nieminen P, Guatelli S and Incerti S 2019 Evaluation of early radiation DNA damage in a fractal cell nucleus model using Geant4-DNA Phys. Medica 62 152–7 Online: 10.1016/j.ejmp.2019.04.010

Sanguanmith S, Meesungnoen J and Jay-Gerin JP 2013 Time-dependent yield of OH radicals in the low linear energy transfer radiolysis of water between 25 and 350 °C Chem. Phys. Lett 588 82–6 Online: 10.1016/j.cplett.2013.09.057

Schuemann J, McNamara AL, Ramos-Méndez J, Perl J, Held KD, Paganetti H, Incerti S and Faddegon B 2018 TOPAS-nBio: An Extension to the TOPAS Simulation Toolkit for Cellular and Sub-cellular Radiobiology Radiat. Res 191 125 Online: http://www.rrjournal.org/doi/pdf/10.1667/RR15226.1

Shin W-G, Ramos-Mendez J, Faddegon B, Tran HN, Villagrasa C, Perrot Y, Okada S, Karamitros M, Emfietzoglou D, Kyriakou I, Bordage MC, Sakata D, Guatelli S, Choi HJ, Min CH, Lee SB and Incerti S 2019 Evaluation of the influence of physical and chemical parameters on water radiolysis simulations under MeV electron irradiation using Geant4-DNA J. Appl. Phys 126 114301 Online: http://aip.scitation.org/doi/10.1063/1.5107511

Shin WG, Bordage MC, Emfietzoglou D, Kyriakou I, Sakata D, Min CH, Lee SB, Guatelli S and Incerti S 2018 Development of a new Geant4-DNA electron elastic scattering model for liquid-phase water using the ELSEPA code J. Appl. Phys 124 Online: 10.1063/1.5047751

Shiraishi H, Katsumura Y, Hiroishi D, Ishigure K and Washio M 1988 Pulse-radiolysis study on the yield of hydrated electron at elevated temperatures J. Phys. Chem 92 3011–7 Online: http://pubs.acs.org/doi/abs/10.1021/j100321a061

Shweta H and Sen S 2018 Dynamics of water and ions around DNA: What is so special about them? J Biosci 43 499–518 [PubMed: 30002269]

Štěpán V and Davídková M 2014 RADAMOL tool: Role of radiation quality and charge transfer in damage distribution along DNA oligomer Guest editors: Solov'yov Andrey V, Mason Nigel, Limão-Vieira Paulo, Smialek-Telega Malgorzata Eur. Phys. J. D 68

Sultana A, Meesungnoen J and Jay-Gerin JP 2020 Yields of primary species in the low-linear energy transfer radiolysis of water in the temperature range of 25–700 °c Phys. Chem. Chem. Phys 22 7430–9 [PubMed: 32215415]

Tachiya M 1983 Theory of diffusion-controlled reactions: Formulation of the bulk reaction rate in terms of the pair probability Radiat. Phys. Chem 21 167–75 Online: https://linkinghub.elsevier.com/retrieve/pii/0146572483901437

Tomita H, Kai M, Kusama T and Aoki Y 1995 Strand Break Formation in Plasmid DNA Irradiated in Aqueous Solution: Effect of Medium Temperature and Hydroxyl Radical Scavenger Concentration. J. Radiat. Res 36 46–55 Online: https://academic.oup.com/jrr/article-lookup/doi/10.1269/jrr.36.46 [PubMed: 7616487]

Tomita H, Kai M, Kusama T and Ito A 1998 Monte Carlo simulation of DNA strand-break induction in supercoiled plasmid pBR322 DNA from indirect effects Radiat. Environ. Biophys 36 235–41 Online: http://link.springer.com/10.1007/s004110050077 [PubMed: 9523339]

Tomita H, Kai M, Kusama T and Ito A 1997 Monte Carlo simulation of physicochemical processes of liquid water radiolysis Radiat. Environ. Biophys 36 105–16 Online: http://link.springer.com/10.1007/s004110050061 [PubMed: 9271798]

Tran HN, Ramos-Méndez J, Shin W, Perrot Y, Faddegon B, Okada S, Karamitros M, Davídková M, Štěpán V, Incerti S and Villagrasa C 2021 Assessment of DNA damage with an adapted independent reaction time approach implemented in Geant4-DNA for the simulation of diffusion-controlled reactions between radio-induced reactive species and a chromatin fiber Med. Phys 48 890–901 Online: https://onlinelibrary.wiley.com/doi/10.1002/mp.14612 [PubMed: 33232522]

Udovičić L, Mark F, Bothe E and Udovicic L 1994 Yields of Single-Strand Breaks in Double-Stranded Calf Thymus DNA Irradiated in Aqueous Solution in the Presence of Oxygen and Scavengers Radiat. Res 140 166 Online: https://www.jstor.org/stable/3578899?origin=crossref [PubMed: 7938464]

Uehara S and Nikjoo H 2006 Monte Carlo simulation of water radiolysis for low-energy charged particles. J. Radiat. Res 47 69–81 [PubMed: 16571920]

Vologodskii AV and Cozzarelli NR 1994 Conformational and thermodynamic properties of supercoiled DNA Annu. Rev. Biophys. Biomol. Struct 23 609 [PubMed: 7919794]

Wang F, Schmidhammer U, Larbre JP, Zong Z, Marignier JL and Mostafavi M 2018 Time-dependent yield of the hydrated electron and the hydroxyl radical in D2O: A picosecond pulse radiolysis study Phys. Chem. Chem. Phys 20 15671–9 [PubMed: 29845125]

Wardman P. 2020; Radiotherapy Using High-Intensity Pulsed Radiation Beams (FLASH): A Radiation-Chemical Perspective. Radiat. Res. 194

Yanisch-Perron C, Vieira J and Messing J 1985 Improved M13 phage cloning vectors and host strains: nucleotide sequences of the M13mpl8 and pUC19 vectors Gene 33 103–19 Online: https://linkinghub.elsevier.com/retrieve/pii/0378111985901209 [PubMed: 2985470]

Zhu H, McNamara AL, McMahon SJ, Ramos-Mendez J, Henthorn NT, Faddegon B, Held KD, Perl J, Li J, Paganetti H and Schuemann J 2020a Cellular Response to Proton Irradiation: A Simulation Study with TOPAS-nBio Radiat. Res 194 9 Online: http://www.rrjournal.org/doi/10.1667/RR15531.1 [PubMed: 32401689]

Zhu H, McNamara AL, Ramos-Mendez J, McMahon SJ, Henthorn NT, Faddegon B, Held KD, Perl J, Li J, Paganetti H and Schuemann J 2020b A parameter sensitivity study for simulating DNA damage after proton irradiation using TOPAS-nBio Phys. Med. Biol 65 085015 Online: https://iopscience.iop.org/article/10.1088/1361-6560/ab7a6b [PubMed: 32101803]

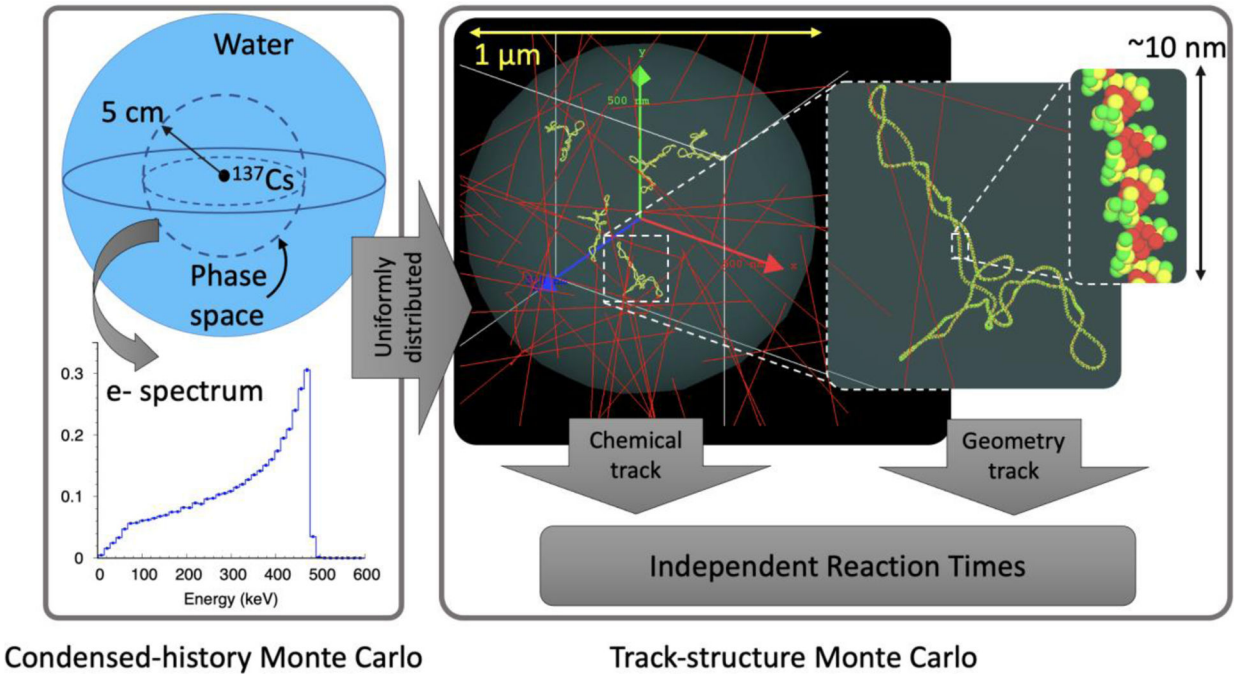

Figure 1.

Setup showing a two-stage simulation. The condensed-history MC simulation setup used to retrieve the secondary electron spectrum is shown on the left side. The track-structure MC simulation setup used to calculate SSB and DSB yields using supercoiled plasmid DNA is shown on the right side. Red lines correspond to few electron tracks. For more details, see the text.

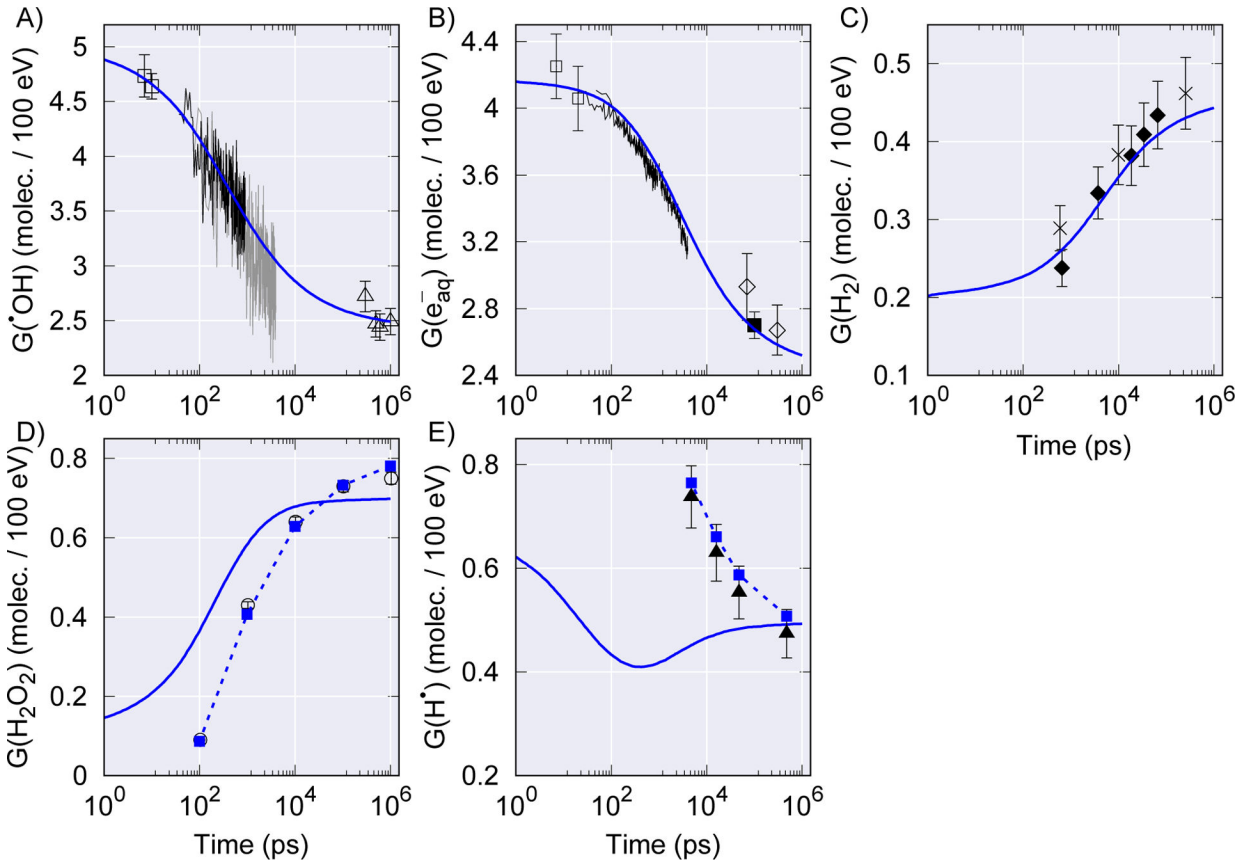

Figure 2.

Time-dependent G values for fast electrons (1 molec./100 eV = 1.036×10^{-7} mol J^{-1}). TOPAS-nBio/Geant4-DNA simulated data: (solid line) pure liquid water calculations; (blue squares connected with dashed lines) simulations of scavenger systems for H_2O_2 and $H^{\bullet}$ as shown in table 1. Error bars represent statistical uncertainties, one standard deviation. Measured data: black and grey solid lines (Ma et al 2015); □ (Wang et al 2018); △ (Laverne 2000); ■ (Bartels et al 2000); ◇ (Shiraishi et al 1988); × and ◆ (Pastina et al 1999); ○ (Hiroki et al 2002); ▲ (Huerta Parajon et al 2008).

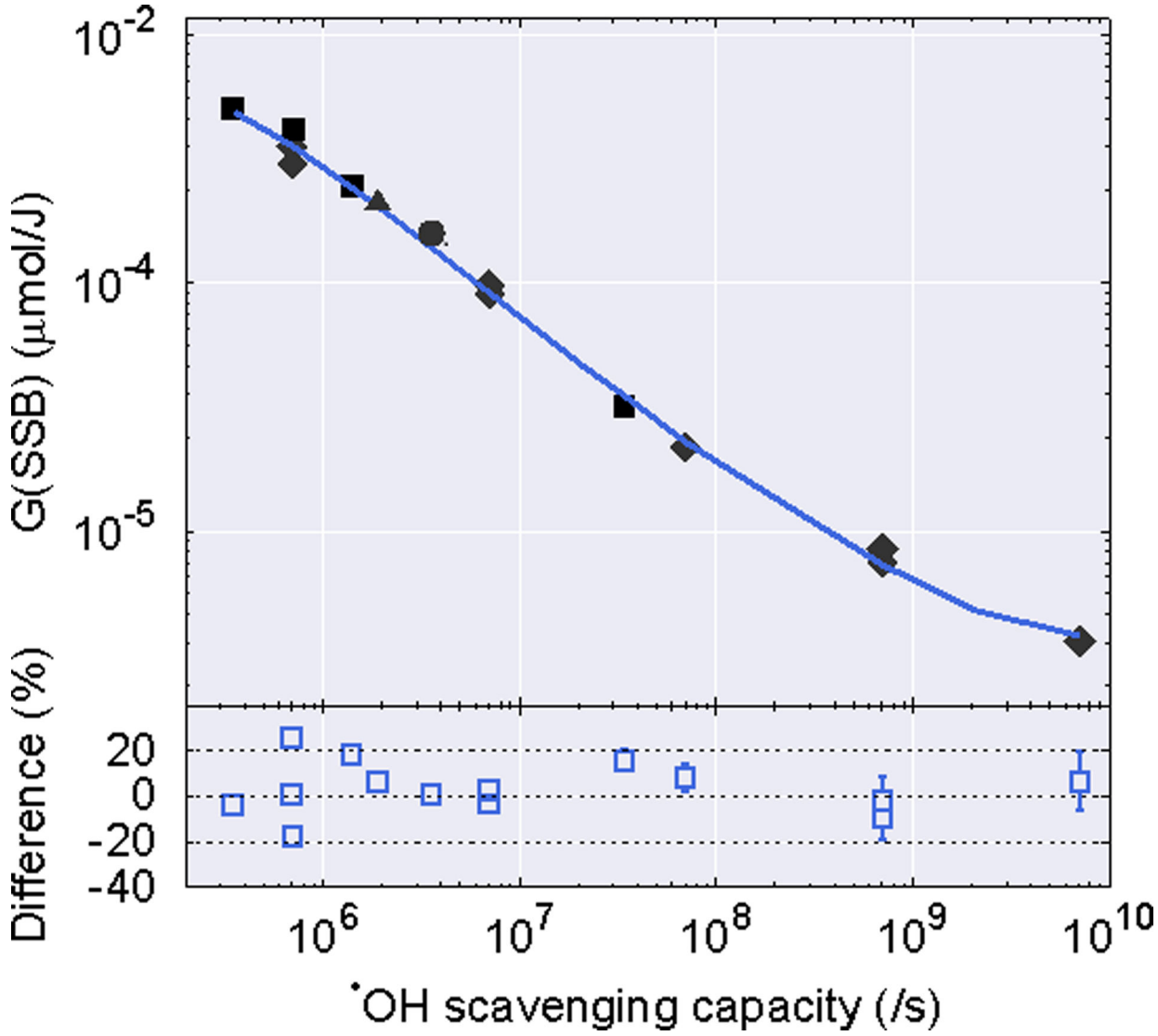

Figure 3.

Total calculated SSB yields (direct plus indirect) as a function of •OH scavenging capacity (solid lines). Measured data for pUC18 is from ■ (Milligan et al 1993), ◆ (Milligan and Ward 1994), and ● (Milligan et al 1996). Measured data for pUC19 ▲ is from (Perry et al 2021). Percentage differences (□) between calculated to measured data are shown in the bottom figure. The dotted lines are margins from experimental uncertainty. Error bars are displayed when bigger than the symbol, represent statistical uncertainties from Monte Carlo simulations, one standard deviation.

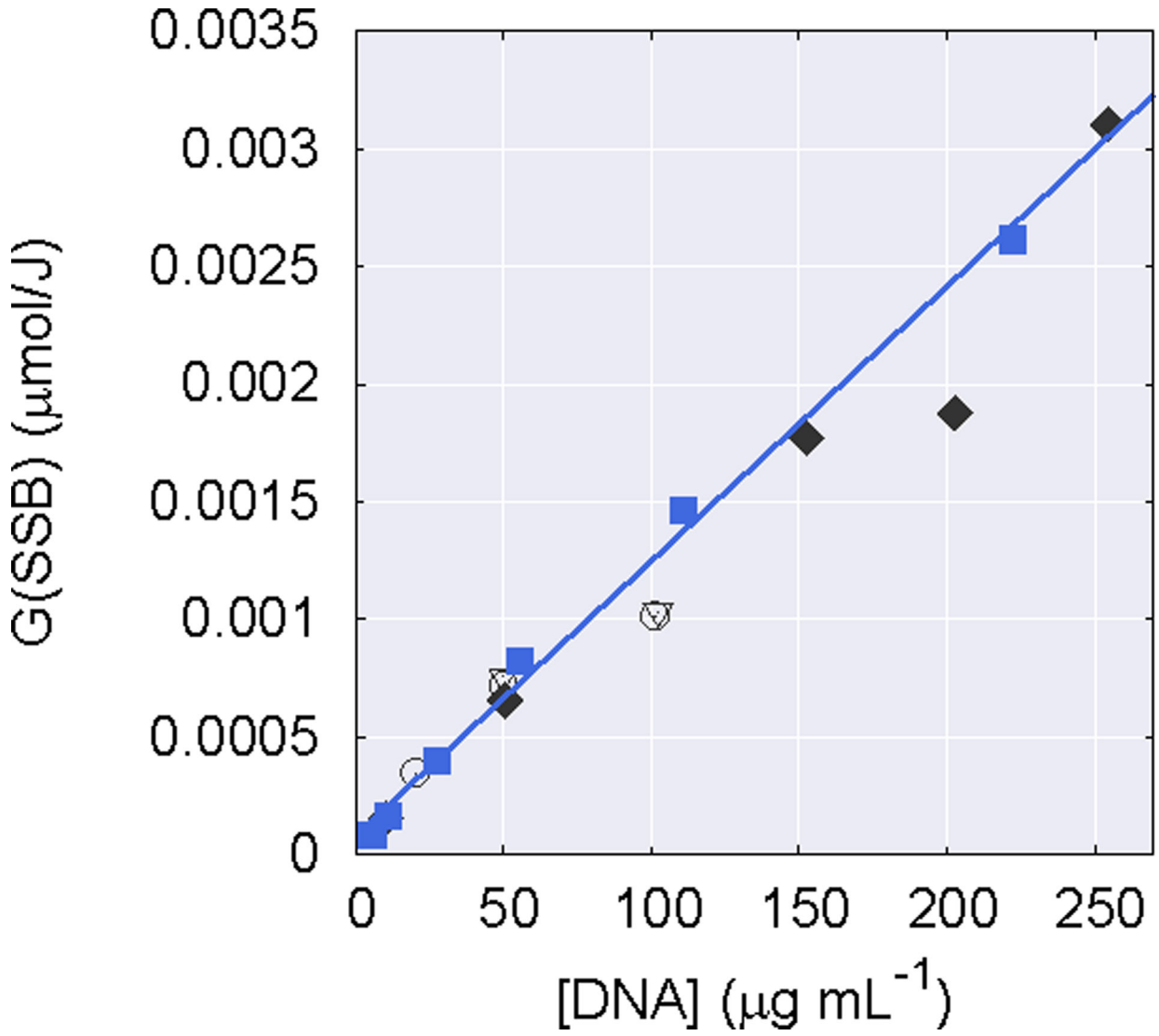

Figure 4.

Calculated G(SSB) as a function of the DNA concentration (■ connected with solid line). Error bars, smaller than the symbols, represent statistical uncertainties, one standard deviation. Measured data is from (Milligan et al 1993): pUC18 (○); pEC (△); and SV40 (◆).

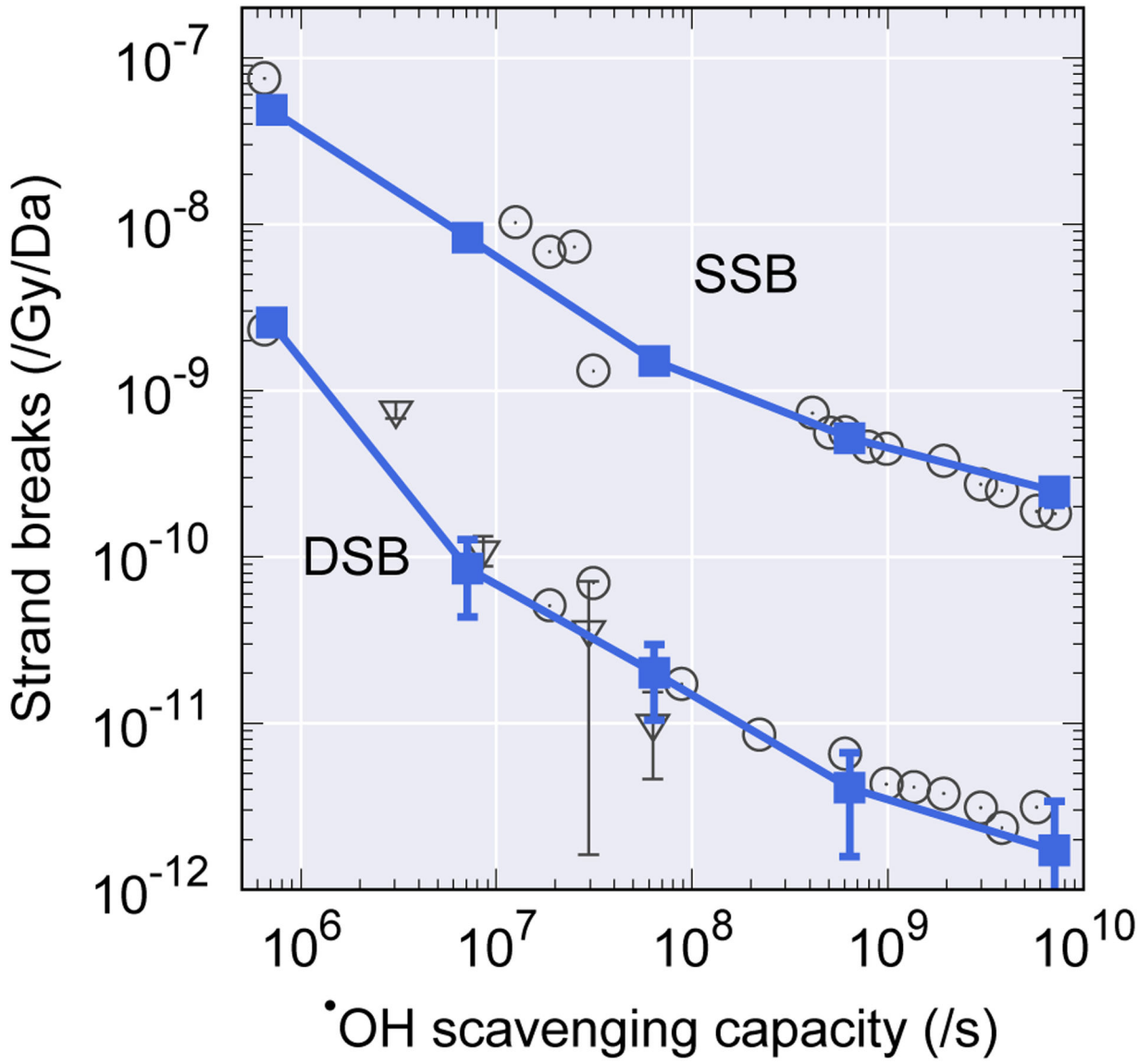

Figure 5.

Calculated single and double-strand break yields as a function of hydroxyl radical scavenging capacity. Error bars represent statistical uncertainties, one standard deviation. Measured data: ○ pBR322 (Klimczak et al 1993), ∇ pBR322 (Tomita et al 1995).

Table 1

List of reaction rate constants used for the simulation of G values obtained from (Buxton et al 1988) (Milligan et al 1996) (Pastina and LaVerne 1999) and (Huerta Parajon et al 2008)

Reactions for simulation of radiolysis in pure liquid water.	
Reaction	k_{obs} (/M/s)
$e^-_{aq} + e^-_{aq} \rightarrow H_2 + OH^-$	5.5×10^9
$e^-_{aq} + H_3O^+ \rightarrow H^\bullet$	2.3×10^{10}
$e^-_{aq} + H^\bullet \rightarrow H_2 + OH^-$	2.5×10^{10}
$e^-_{aq} + {}^\bullet OH \rightarrow OH^-$	3.0×10^{10}
$e^-_{aq} + H_2O_2 \rightarrow OH^- + {}^\bullet OH$	1.1×10^{10}
$H_3O^+ + OH^- \rightarrow H_2O$	14.3×10^{10}
$H^\bullet + H^\bullet \rightarrow H_2$	7.8×10^9
$H^\bullet + {}^\bullet OH \rightarrow H_2O$	1.55×10^{10}
$H^\bullet + H_2O_2 \rightarrow {}^\bullet OH + H_2O$	9.0×10^7
${}^\bullet OH + {}^\bullet OH \rightarrow H_2O_2$	5.5×10^9

Reactions with scavengers for DNA damage simulation.	
Reaction	**k_{obs} (/M/s)**
$e^-_{aq} + O_2 \rightarrow O_2^-$	1.9×10^{10}
$H^\bullet + O_2 \rightarrow HO_2$	2.1×10^{10}
${}^\bullet OH + DMSO$	7.1×10^9
$H^\bullet + DMSO$	2.7×10^6
$e^-_{aq} + DMSO$	3.8×10^6

Reactions for calculating G(H_2O_2)	
Reaction	**k_{obs} (/M/s)**
$CH_3OH + {}^\bullet OH \rightarrow {}^\bullet CH_2OH + H_2O$	9.7×10^8
$NO_3^- + e_{aq}^- \rightarrow {}^\bullet NO_3^{2-}$	9.7×10^9
$NO_3^- + {}^\bullet H \rightarrow {}^\bullet NO_3^{2-}$	1.4×10^6

Reactions with DNA	
Reaction	**k_{obs} (/M/s)**
${}^\bullet OH + DNA$	Variable
$H^\bullet + DNA$	0.03×10^9
$e^-_{aq} + DNA$	0.01×10^9

Reactions for calculating G($H^\bullet$)	
Reaction	**k_{obs} (/M/s)**
${}^\bullet H + HCO_2^- \rightarrow H_2 + {}^\bullet CO_2^-$	2.1×10^8
$e^-_{aq} + NO_3^- \rightarrow NO_3^{2-}$	9.7×10^9
$Br + {}^\bullet OH \rightarrow$	1.1×10^{10}

Table 2

Displacements of physical and dissociation products implemented in Geant4-DNA.

Physical product	Dissociation products	$RMS^{H_2O^+}$ or $RMS^{H_2O^*}$	Displacement	
H_2O^+	$H_3O^+ + {}^\bullet OH$ [1]	2.0 nm	H_3O^+ $^\bullet OH$	0 or 0.8 nm [2] 0.8 or 0 nm [2]
H_2O^*	$H^\bullet + {}^\bullet OH$	2.4 nm	$H^\bullet$ $^\bullet OH$	17/18 $RMS^{H_2O^*}$ 1/18 $RMS^{H_2O^*}$
	$H_2 + 2\ {}^\bullet OH$	0.8 nm	H_2 $^\bullet OH$ $^\bullet OH$	2/18 $RMS^{H_2O^*}$ 16/18 $RMS^{H_2O^*}$ + 0.55 nm 16/18 $RMS^{H_2O^*}$ + 0.55 nm [3]
	$H_2 + {}^\bullet OH + OH^-$	0.8 nm	H_2 $^\bullet OH$ OH^-	2/18 $RMS^{H_2O^*}$ 16/18 $RMS^{H_2O^*}$ + 0.55 nm 16/18 $RMS^{H_2O^*}$ + 0.55 nm [3]

[1] If e^-_{aq} are produced after an autoionization event, then its position is sampled using the one-step thermalization model. See the text.

[2] Either value is selected randomly with 50% probability.

[3] Positioned in the opposite direction from the first $^\bullet OH$